VPR Adjustment using a Dual CAPPI Technique

Iwan Holleman[1]

[1]Royal Netherlands Meteorological Institute (KNMI), P.O. Box 201, NL-3730 AE De Bilt, The Netherlands

Manuscript submitted to

ERAD Publication Series

Manuscript-No. ERAD3-P-00021

Offset requests to:
I. Holleman
KNMI, P.O. Box 201, NL-3730 AE De Bilt, The Netherlands

ERAD Publication Series (2004) 0000:0001–6

VPR Adjustment using a Dual CAPPI Technique

Iwan Holleman[1]

[1]Royal Netherlands Meteorological Institute (KNMI), P.O. Box 201, NL-3730 AE De Bilt, The Netherlands

Abstract. A straightforward technique for VPR adjustment based on the analysis of accumulated pseudoCAPPI data at two different heights is proposed. The extracted VPR gradient is used to perform a range and azimuth dependent adjustment using a purely analytical expression. The application of the dual-CAPPI technique is illustrated using a case of stratiform precipitation and a strong bright band interference. A preliminary verification indicates that the dual-CAPPI technique performs rather good for cases with stratiform precipitation. The development of the dual-CAPPI technique will be continued by a semi-operational implementation and a more detailed verification.

1 Introduction

The Vertical Profile of Reflectivity (VPR) is, especially at higher latitudes, the major source of error in quantitative precipitation estimates deduced from radar observations (Joss and Waldvogel, 1990; Koistinen, 1991). Many different techniques have therefore been developed to estimate the vertical profile of reflectivity and to subsequently correct the radar precipitation estimates for this profile. The vertical profile of reflectivity can be estimated using climatological profiles, mean reflectivity profiles or local profiles obtained at short ranges (Vignal et al., 2000; Vignal and Krajewski, 2001; Koistinen et al., 2003). Alternatively, the VPR can be determined using a sophisticated technique based on inverse theory (Andrieu and Creutin, 1995; Vignal et al., 1999). Kitchen et al. (1994) have developed a method to assign an idealized VPR profile to each radar pixel based on satellite derived cloud top height, model freezing level height, and orographic contribution dependent on model winds.

On the other hand, gauge adjustment techniques have been developed which amongst others correct the radar precipitation estimates using a second-order polynomial in range, e.g. Michelson et al. (2000). Because the height of the radar beam increases approximately quadratic with range, these gauge adjustment techniques basically correct for a gradient in the vertical profile of reflectivity.

In a flat country, like the Netherlands, application of the sophisticated VPR adjustment techniques may be overdone because at 150 km range a translation from 2 km altitude down to ground level is needed, which is actually within the radar beam width at that range. It is therefore expected that the main effect of the VPR on the radar precipitation estimates can be described by a gradient parameter only, just like it is implicitly done in some gauge adjustment techniques. Here we present a straightforward technique for VPR adjustment of radar precipitation estimates using pseudoCAPPI data at two different altitudes. PseudoCAPPIs with target altitudes of 0.8 and 1.8 km are produced from 4-elevation volume scans every 5 minutes and are accumulated over 3-hourly and daily periods. The gradient in vertical profile of rainfall is then determined from the two accumulations obtained at the different target altitudes. The adjustment factor as a function of range for the lower pseudoCAPPI accumulation, including the gradient effect and beam broadening, is described by an analytical expression.

In this paper the theoretical details of the dual CAPPI technique will be highlighted first. Using a case of stratiform precipitation and a strong bright band, the application of the dual CAPPI technique will be discussed step-by-step, and the stability of the deduced gradient and the effect of bright band interference will be shown. Finally a quantitative assessment of the adjusted radar precipitation estimates is made by comparison with daily gauge accumulations, and preliminary results from this verification will be presented together with an outlook.

2 Description of the Dual CAPPI technique

The KNMI radars in De Bilt and Den Helder perform a 4-elevation reflectivity scan every 5 minutes. From these scans pseudoCAPPI images are produced with a spatial resolution

Correspondence to: I. Holleman (holleman@knmi.nl)

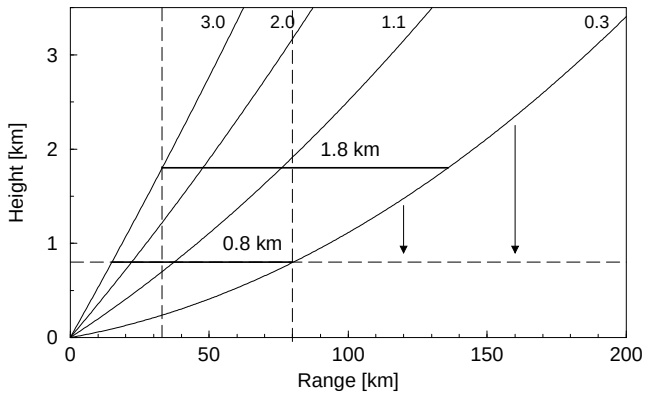

Fig. 1. This figure shows the calculated height of the radar beam as a function of range for all elevations in the volume scan. The ranges where the 0.8 and 1.8 km CAPPIs can be calculated are marked by the bold horizontal lines and the overlap region is indicated by the dashed vertical lines. The vertical arrows symbolize the adjustment of data aloft in order to represent the precipitation intensity at the target height (horizontal dashed line).

of 2.5 km and a target height of 0.8 and 1.8 km above antenna level. Ground clutter is removed from the pseudo-CAPPI images using a stepwise procedure based on a statistical method (Wessels and Beekhuis, 1997). The reflectivity values are converted to rainfall intensities using a fixed Z-R relationship, $Z = 200R^{1.6}$. In this way, 3-hour accumulations are produced every hour and 24-hour accumulations are produced at 08 UTC.

The radar estimates of the accumulated precipitation (3-hour or 24-hour) based on the pseudoCAPPI images with target heights of $z_l = 0.8$ km and $z_u = 1.8$ km above antenna level are primary input for the dual-CAPPI adjustment. In figure 1 the calculated beam height as a function of range is shown for the four elevations used to construct the pseudo-CAPPI images. These four elevations are 0.3, 1.1, 2.0 and 3.0 degrees. The two solid horizontal lines in the figure mark the regions where reflectivity values at the CAPPI target heights can be obtained by interpolation of the data at the different elevations. It can be seen that the target height of the lowest pseudoCAPPI can be reached up to a range of 80 km only. At longer ranges the height of observation will increase and in the presence of a significant gradient in the vertical profile of reflectivity, this will give rise to the well-known increasing underestimation of the accumulated precipitation with increasing range.

In figure 1 the region where both pseudoCAPPI images can be interpolated to their target heights, i.e., the true CAPPI regions, has been marked by the two vertical dashed lines. This doughnut-shaped region ranges from 33 to 80 km from the radar site. The observations in this region are used to estimate the gradient of the vertical profile of reflectivity between the two target heights. For this an exponential form of the precipitation intensity with height is assumed:

$$R(z) = R_0 \exp[z/\tilde{G}] \tag{1}$$

$$G = 10\,\tilde{G}/\ln 10 \tag{2}$$

where $R(z)$ represents the observed accumulated precipitation in mm at height z and G the gradient in the vertical profile of rainfall intensity in dBR/km. Note that G is a factor of b (exponent in Z-R relationship) smaller than the corresponding VPR gradient in dBZ/km. Assuming that the gradient $\tilde{G}$ is constant within a certain area A, it can be estimated using the following equation:

$$\tilde{G} = \frac{1}{z_u - z_l}\,\ln\left[\frac{\sum_{(i,j)\,\in A} R_u(i,j)}{\sum_{(i,j)\in A} R_l(i,j)}\right] \tag{3}$$

where $R_u(i,j)$ and $R_l(i,j)$ are the accumulated precipitation at pixel (i,j) from the upper and lower pseudoCAPPI images, respectively. In this way the gradient can be calculated for the whole doughnut region or for certain azimuthal sectors.

The VPR gradient G estimated in a certain azimuthal sector is used to adjust the accumulated precipitation obtained at longer ranges. In figure 1, the two arrows symbolize the adjustment of the precipitation accumulations beyond the "true" CAPPI region of the lower pseudoCAPPI images to the target height z_l. In this way the range dependent bias within the radar-based precipitation accumulation products is removed.

To calculate the adjustment factor as a function of range from the VPR gradient G, one has to consider the shape of the radar beam f:

$$f(z, \hat{z}_x, \Delta z) = f_0 \exp[-4 \ln 2\ (z - \hat{z}_x)^2/\Delta z^2] \tag{4}$$

where z is the height, $\hat{z}_x$ is the pseudoCAPPI height with $x \in (u, l)$, and Δz is the beam width in km. The pseudo-CAPPI height is equal to the target height in the true CAPPI region, and it follows the highest and lowest elevation at shorter and longer ranges, respectively (see figure 1). The observed precipitation accumulation $\tilde{R}$ can now be modeled as a function of range and target height using equations 1 and 4:

$$\tilde{R}(\hat{z}_x, \Delta z) \equiv \int_0^\infty R(z) \cdot f(z, \hat{z}_x, \Delta z)^{2/b}\, dz \tag{5}$$

where the range enters the equation implicitly via the pseudoCAPPI height and the beam width. The modeled accumulation is basically a beam shape weighted average of the precipitation intensity with height. The $2/b$-exponent of the beam shape in the equation reflects the double occurrence of the beam shape in the radar equation (Doviak and Zrnić, 1993) and the non-linear relationship between reflectivity and precipitation intensity. Using equations 1 and 4 the modeled precipitation accumulation can be written as:

$$\tilde{R}(\hat{z}_x, \delta z) = \tilde{R}_0\ \exp\left[\tilde{G} \cdot \hat{z}_x + (\frac{\tilde{G} \cdot \delta z}{2})^2\right] \times \\ \times\ \mathrm{erfc}\left[-\frac{\hat{z}_x}{\delta z} - \frac{\tilde{G} \cdot \delta z}{2}\right] \tag{6}$$

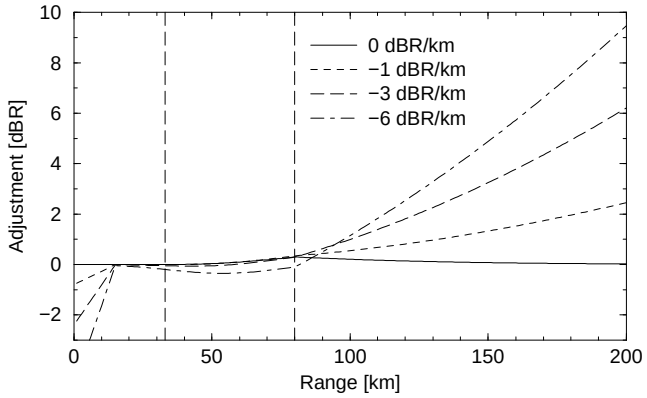

Fig. 2. This figure shows the simulated adjustment factor as a function of range using an initial VPR gradient of 0, -1, -3, and -6 dBR/km. The overlap region between the 0.8 and 1.8 km CAPPIs is indicated by the dashed vertical lines. The parameters used for the simulation are listed in table 1.

where $\tilde{R}_0$ is an arbitrary constant. The "erfc" refers to the complementary error function (Press et al., 1992) and the scaled beam width δz is defined as:

$$\delta z \equiv \sqrt{\frac{b}{8 \ln 2}}\, \Delta z \tag{7}$$

which is only introduced to make the previous equation easier to read.

The modeled precipitation accumulation as a function of height and beam width can be used to derive an expression for the adjustment factor as a function of range and the observed VPR gradient. The adjustment factor F is defined as the ratio between the modeled accumulation at target height z_l and $\delta z = 0$ (dashed horizontal line in fig 1) and that for the lowest pseudoCAPPI:

$$F(z_l) \equiv \frac{R(z_l, 0)}{R(\hat{z}_l, \delta z)} = \frac{2\, \tilde{R}_0\, \exp[\tilde{G} \cdot z_l]}{\tilde{R}(\hat{z}_l, \delta z)} \tag{8}$$

where the following property of the complementary error function has been used: $\mathrm{erfc}(-\infty) = 2$ (Press et al., 1992). The modeled adjustment factor as a function of range for several VPR gradients are plotted in figure 2. It is evident from the figure that in absence of a VPR gradient hardly any adjustment is done, while the adjustment becomes significant (up to 10 dBR) for the larger gradients and longer ranges. For larger gradients (e.g. -6 dBR/km) an attenuation at short ranges (< 80 km) is observed which compensates for the inhomogeneous beam filling caused by the VPR gradient. The parameters used to calculate these adjustment factor curves are listed in table 1.

Table 1. This table lists the parameters used to calculate the VPR adjustment factor as a function of range.

Parameter	Value
Elevations	0.3, 1.1, 2.0, 3.0 degrees
Lower pseudoCAPPI	0.8 km
Upper pseudoCAPPI	1.8 km
Angular beam width	1.0 degree
Z-R exponent b	1.6
4/3 earth's radius	8495 km

In the following section, the ratio between accumulated precipitation from the lower and upper pseudoCAPPI images will be analyzed as a function of range. Using the equation for the modeled precipitation accumulation, this ratio R_{ul} can be expressed as:

$$R_{ul} \equiv \frac{R(\hat{z}_u, \delta z)}{R(\hat{z}_l, \delta z)} \tag{9}$$

where the range dependence is again implicitly in the pseudoCAPPI height $\hat{z}_x$ and the radar beam width.

3 Results

In figure 3 two radar images with the accumulated precipitation between 08 UTC 12 January 2004 and 08 UTC 13 January 2004 are shown. This period contained an episode of significant stratiform precipitation caused by the subsequent passage of a warm front and an occlusion front. The radar is located in De Bilt (5.17E,52.10N) which is in the center of The Netherlands and the antenna is mounted at a height of 44 m above mean sea level. From the 12 UTC 12 January 2004 radiosonde launch at De Bilt, the height of the 0° Celsius isotherm was determined to be 0.80 km. The accumulation period matches that of the climatological rain gauges of KNMI which report daily at 08 UTC. This network consists of about 325 stations and it has a density of roughly 1 station per 100 km^2. The accumulated precipitation observed by this climatological network will be used for verification of the dual-CAPPI adjustment technique. The left image of the figure shows the accumulated precipitation determined using the lower pseudoCAPPIs (0.8 km) and the right image is determined using upper pseudoCAPPIs (1.8 km). Note that the bright band is clearly visible in the right image at short range (13 km) from the radar, i.e, within the smallest circle. In the left image a maximum accumulation of roughly 23 mm is observed while at the same location in the right image an accumulation of only 9 mm is seen. This large difference between the accumulations deduced from the lower and upper pseudoCAPPIs and the evident decrease of the observed values with increasing range are clearly due to the vertical profile of reflectivity.

The gradient in the vertical profile of rainfall intensity is estimated from lower and upper pseudoCAPPI accumulations shown in figure 3 using equation 3. The gradient is determined as a function of azimuth within the doughnut-shaped overlap region of the lower and upper CAPPIs using azimuthal bins of 1, 30, and 360 degrees. For this the azimuth

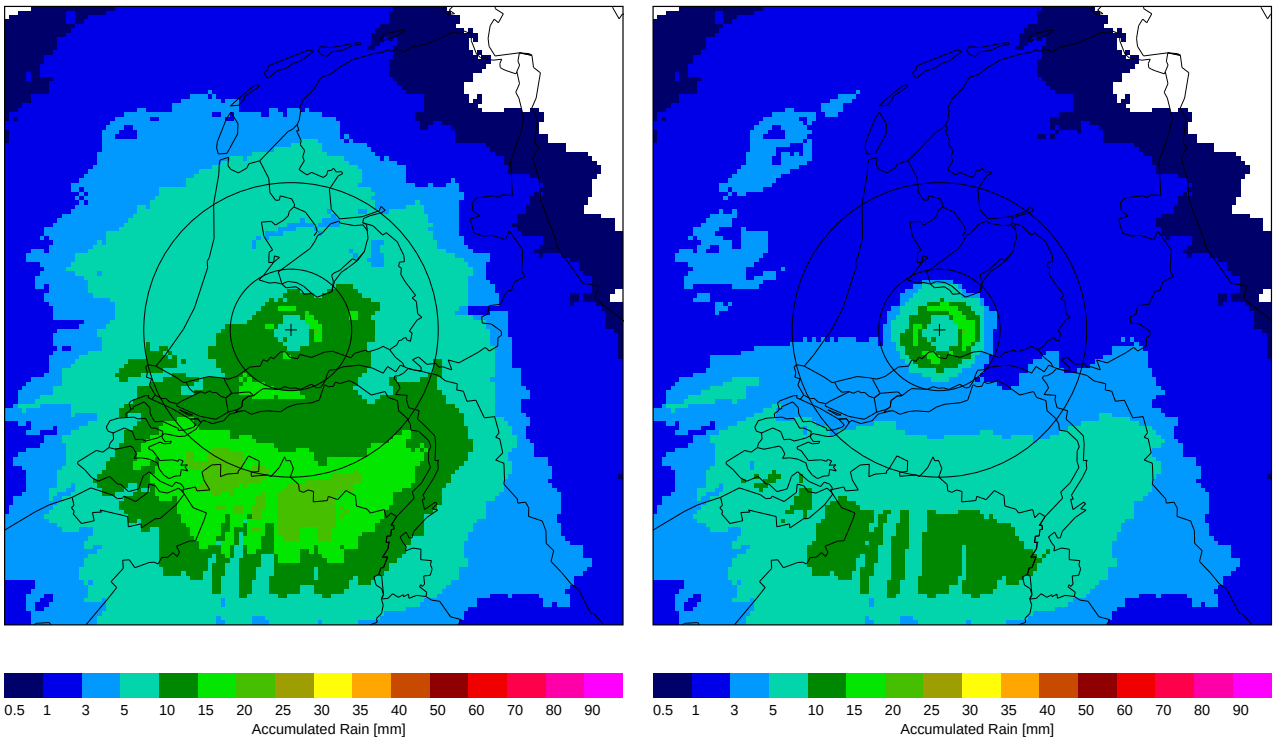

Fig. 3. This figure shows two images with the accumulated precipitation from 08 UTC 12 January 2004 till 08 UTC 13 January 2004 as observed by the radar in De Bilt (marked with a cross). The left accumulation is determined using pseudoCAPPIs at 0.8 km altitude and the right accumulation using pseudoCAPPIs at 1.8 km altitude. The doughnut-shaped overlap region between the 0.8 and 1.8 km CAPPIs is indicated by two circles (radii of 33 and 80 km) centered at the radar site.

and range with respect to the radar of each pixel in the Cartesian image are reconstructed using the azimuthal equidistant projection. In figure 4 the obtained VPR gradient is plotted as a function of azimuth for the 3 different bin sizes. It is evident from the figure that the gradient G is rather stable over the analyzed domain. At 1 degree azimuthal resolution the noise on the gradient is only a few tenths of dB (apart from a few spikes). The 30 degree running average is rather smooth but shows a clear dip in easterly direction. The absolute value of the gradient in the vertical profile of rainfall intensity varies roughly between -6.5 and -4.5 dBR/km. The 360-degree averaged gradient is -4.89 dBR/km, which corresponds to a VPR gradient of -7.8 dBZ/km. The observed VPR gradient falls within the range of values, -7.5 to -12 dBZ/km, reported by Koistinen (1991) for the snowfall gradient above the bright band.

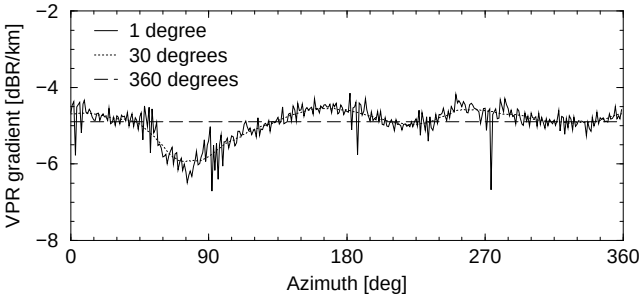

Fig. 4. This figure shows the VPR gradient as a function of azimuth as determined in the overlap region of the 0.8 and 1.8 km CAPPIs from figure 3 using 1, 30, and 360 degree bins.

The (ratio between the) lower and upper pseudoCAPPI accumulations of figure 3 can be analyzed as a function range from the radar. For both accumulations the mean precipitation accumulation is calculated as a function of range using 1 km range bins. The result is depicted in figure 5. The upper frame of the figure shows the mean accumulated precipitation for both the lower and the upper pseudoCAPPIs as a function of range and the lower frame shows the ratio between the lower and upper pseudoCAPPI accumulations as a function of range. The two curves in the upper frame are overlapping at short range and at long range, and in between they exhibit some pronounced features. The curve for the upper pseudoCAPPI shows a sharp peak at 13 km range and a broad feature with a long tail around 120 km range, while the curve for lower pseudoCAPPI shows two sharp peaks and a broader peak with again a long tail. For all elevations, the calculated range where the radar beam crosses the height of the 0° Celsius isotherm (0.80 km) is marked in the figure by a bar. It is evident that most features in the two curves can be attributed to bright band amplification of

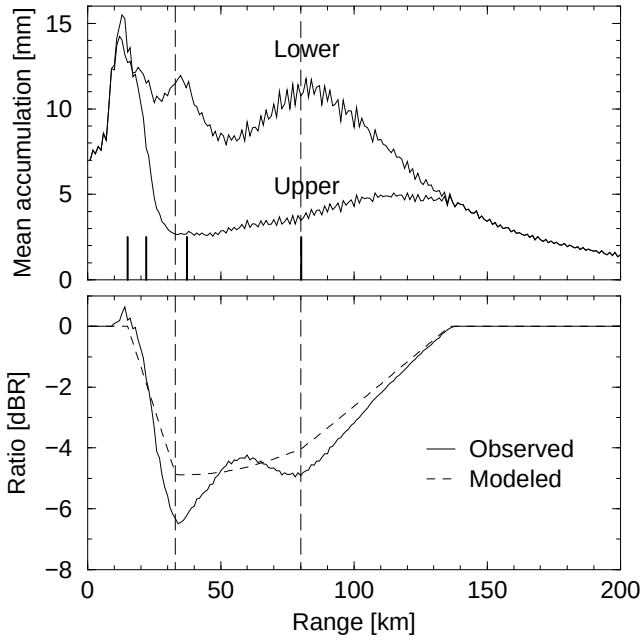

Fig. 5. The upper frame of this figure shows the mean precipitation accumulation as a function of range for the upper and lower pseudoCAPPI accumulations of figure 3. The mean accumulation has been calculated by averaging of all pixel values over all azimuths using a 1 km range bin. The bars mark the range where the beam crosses the height of the 0° Celsius isotherm on 12 UTC 12 January 2004 (0.80 km) for all elevations. The lower frame shows the observed and modeled ratio between the upper and lower pseudoCAPPI accumulations as a function of range. The model curve has been calculated using a VPR gradient of -4.89 dBR/km.

the radar returns. In accordance with expectations the bright band features broaden with range due to the smaller elevation angle of the radar beam and to beam broadening. The amplitude of each bright band feature is determined by the pseudoCAPPI weighting factor and thus by the difference between the 0° Celsius isotherm and the pseudoCAPPI height. The broad feature in the curve for the upper pseudoCAPPI is attributed to the southern area with a large precipitation accumulation just outside of the largest circle.

The lower frame of figure 5 shows the ratio between the lower and upper pseudoCAPPI accumulations (solid line) as a function of range. The ratio in dB is zero at short range (< 15 km) and at long range (> 135 km) where both pseudoCAPPIs overlap. One sharp peak and two broader dips which clearly coincide with the bright band features identified in the upper frame of the figure are observed on top of a broad feature. The dashed line represents the ratio between the lower and upper pseudoCAPPI accumulations R_{ul} which is modeled using equation 9 and a VPR gradient of -4.89 dBR/km. This VPR gradient is equal to the 360-degree averaged gradient determined previously for this case. It is evident from the figure that the significant deviations are due to the bright band interferences and that the range-dependent correction is rather insensitive to the overestimation of precipitation in the lower pseudoCAPPI. So a bright band interference can be detected quite well (and possibly also corrected for) using the analysis of the accumulations as a function of range and fortunately the influence of the bright band on the VPR adjustment at long range seems to be limited.

Using the obtained VPR gradient as a function of azimuth and the equation for the adjustment as a function of range (equation 8), all pixels in the precipitation accumulation based on the lower pseudoCAPPIs are adjusted. The 30-degree averaged VPR gradient (see figure 4) has been used for the actual adjustment. The dual-CAPPI adjusted radar accumulation between 08 UTC 12 January 2004 and 08 UTC 13 January 2004 is shown in figure 6. The range of the adjusted radar accumulation is limited to 200 km. Comparing this image with the unadjusted one in the right frame of figure 3 it evident that the observed values at long range have increased substantially and that the increasing underestimation with range has disappeared. The maximum observed accumulation in the southern area has increased to about 32 mm (from 23 mm in the unadjusted image).

The performance of the dual-CAPPI technique has been evaluated quantitatively by verification of the (un)adjusted radar accumulations against those of the climatological rain gauge network of KNMI. The calculated biases and standard deviations are listed in table 2 for 5 days. For all days where the VPR gradient is negative, application of the dual-CAPPI technique results in a moderate-to-large reduction of the bias and/or standard deviation. For the case of convective precipitation, i.e., the day with a positive VPR gradient, application of the dual-CAPPI technique results in a slight increase of the bias. So it appears, in accordance with expectations, that the dual-CAPPI technique performs rather good for stratiform cases and has problems with convective cases. Of course one can decide to only apply the dual-CAPPI adjustment when the VPR gradient is negative.

Table 2. In this table the results of the preliminary verification of the dual-CAPPI adjusted radar accumulations against those of the climatological gauge network. The bias and standard deviation of the radar accumulations before and after adjustment are given in mm. The first column contains the end date of the daily accumulation and the second column the 360-degree averaged VPR gradient in dBR/km.

		Bias		Std. Dev.	
End Date	G_{360}	Before	After	Before	After
13 January 2004	-4.89	-1.6	-0.3	4.6	2.8
30 January 2004	-0.96	-2.1	-1.6	3.0	2.4
01 February 2004	-1.58	-6.4	-4.4	6.0	4.1
07 April 2004	-4.30	-2.2	-1.5	2.1	2.0
03 June 2004	1.79	-0.4	-1.0	3.3	3.3

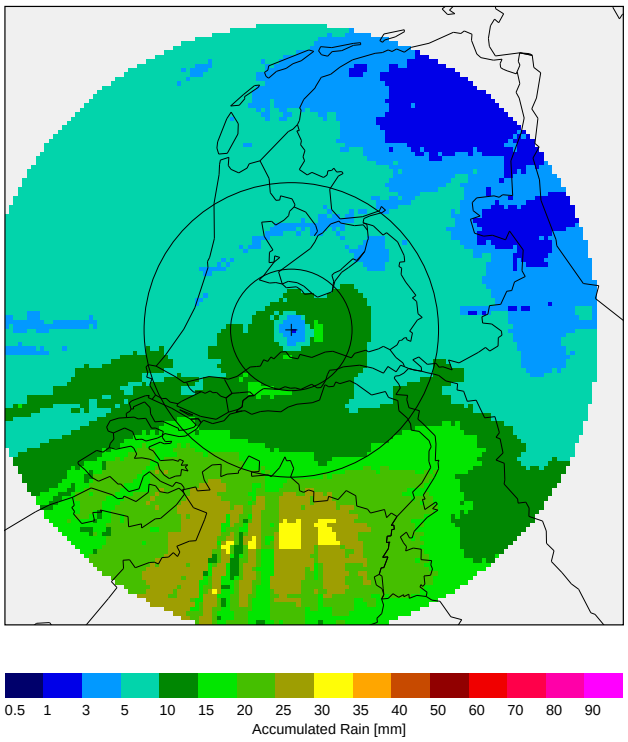

Fig. 6. This image shows the dual-CAPPI-adjusted precipitation accumulation from 08 UTC 12 January 2004 till 08 UTC 13 January 2004. Note that the range of the radar adjusted accumulation is limited to 200 km.

4 Conclusions

A straightforward technique for VPR adjustment of radar precipitation estimates using pseudoCAPPI data at two different altitudes has been presented. Apart from its simplicity, the big advantage for operational implementation of the dual-CAPPI technique is that only accumulated radar data in a Cartesian projection are required. In this paper the theoretical details of the dual CAPPI technique have been highlighted and the analytical equations for the adjustment as a function of range have been introduced. Subsequently the application of the dual CAPPI technique has been discussed step-by-step using a case of stratiform precipitation and a strong bright band. It appeared that the deduced VPR gradient has little noise and is hardly influenced by a strong bright band interference. Furthermore it was found that an analysis of the radar accumulations as a function of range is an excellent tool to detect a bright band interference and can possibly be used to correct for this interference, which will be investigated further. A preliminary verification of the radar accumulations adjusted with the dual-CAPPI technique indicated that the technique performs rather good for stratiform cases. At KNMI, the development of the dual-CAPPI technique will be continued by a semi-operational implementation and a more detailed verification.

Acknowledgements. Hans Beekhuis and Sylvia Barlag are gratefully acknowledged for their feedback and support. This work is done in the framework of the EU COST-717 action “Use of Weather Radar Observations in Hydrological and NWP models”.

References

Andrieu, H. and Creutin, J. D.: Identification of Vertical Profiles of Radar Reflectivity for Hydrological Applications using an Inverse Method. Part I: Formulation, J. Appl. Meteor., 34, 225–239, 1995.

Doviak, R. J. and Zrnić, D. S.: Doppler Radar and Weather Observations, Academic Press, second edn., 1993.

Joss, J. and Waldvogel, A.: Radar in Meteorology, chap. Precipitation Measurement and Hydrology, pp. 577–606, AMS Boston, 1990.

Kitchen, M., Brown, R., and Davies, R. G.: Real-time Corrections of Weather Radar Data for the Effects of Bright Band, Range and Orographic Growth in Widespread Precipitation, Q. J. R. Meteorol. Soc., 120, 1231–1254, 1994.

Koistinen, J.: Operational Correction of Radar Rainfall Errors due to the Vertical Reflectivity Profile, in 25th conference on Radar Meteorology, pp. 91–94, Amer. Meteor. Soc., 1991.

Koistinen, J., Pohjola, H., and Hohti, H.: Vertical Reflectivity Profile Classification and Correction in Radar Composites in Finland, in 31st conference on Radar Meteorology, pp. 534–537, Amer. Meteor. Soc., 2003.

Michelson, D. B., Andersson, T., Koistinen, J., Collier, C. G., Riedl, J., Szrurc, J., Gjertsen, U., Nielsen, A., and Overgaard, S.: BALTEX Radar Data Centre Products and their Methodologies, Report RMK No. 90, Swedish Meteorological and Hydrological Institute (SMHI), 2000.

Press, W. H., Teukolsky, S. A., Vetterling, W. T., and Flannery, B. P.: Numerical Recipes in C: the Art of Scientific Computing, Cambridge University Press, second edn., 1992.

Vignal, B. and Krajewski, W.: Large-Sample Evaluation of Two Methods to Correct Range-Dependent Error for WSR-88D Rainfall Estimates, J. Hydrometeor., 2, 490–504, 2001.

Vignal, B., Andrieu, H., and Creutin, J. D.: Identification of Vertical Profiles of Reflectivity from Volume Scan Radar Data, J. Appl. Meteor., 38, 1214–1228, 1999.

Vignal, B., Galli, G., Joss, J., and Germann, U.: Three Methods to Determine Profiles of Reflectivity from Volumetric Radar Data to Correct Precipitation Estimates, J. Appl. Meteor., 39, 1715–1726, 2000.

Wessels, H. R. A. and Beekhuis, J. H.: Stepwise procedure for suppression of anomalous ground clutter, in COST-75 Seminar on Advanced Radar Systems, pp. 270–277, EUR 16013 EN, 1997.